ELSEVIER

Biophysical Chemistry 113 (2005) 209–221

Biophysical Chemistry

www.elsevier.com/locate/bpc

Review

Nanoscale mechanical and dynamical properties of DNA single molecules

Claudio Anselmi[1], Pasquale DeSantis*, Anita Scipioni

Dipartimento di Chimica, Università di Roma "La Sapienza", I-00185 Rome, Italy

Received 9 July 2004; received in revised form 13 September 2004; accepted 13 September 2004
Available online 18 October 2004

Abstract

Experimental evidence suggests DNA mechanical properties, in particular intrinsic curvature and flexibility, have a role in many relevant biological processes. Systematic investigations about the origin of DNA curvature and flexibility have been carried out; however, most of the applied experimental techniques need simplifying models to interpret the data, which can affect the results.

Progress in the direct visualization of macromolecules allows the analysis of morphological properties and structural changes of DNAs directly from the digitised micrographs of single molecules. In addition, the statistical analysis of a large number of molecules gives information both on the local intrinsic curvature and the flexibility of DNA tracts at nanometric scale in relatively long sequences.

However, it is necessary to extend the classical worm-like chain model (WLC) for describing conformations of intrinsically straight homogeneous polymers to DNA. This review describes the various methodologies proposed by different authors.

Keywords: Persistence length; Worm-like chain; DNA curvature; DNA flexibility; DNA–mica interactions; Divalent cations effects

Contents

1. Introduction . . . 209
2. The worm-like chain model . . . 211
3. DNA persistence length in two dimensions . . . 212
4. Sequence-dependent persistence length . . . 215
5. Mapping DNA curvature and flexibility from SFM images . . . 216
6. Comparison between theoretical and experimental DNA curvature and flexibility . . . 217
7. Recognition effects by the crystal surface . . . 218
8. The effects of cationic metals on the persistence length . . . 219
9. DNA-based nanoarchitectures and nanomotors . . . 219
Acknowledgements . . . 220
References . . . 220

1. Introduction

In the present postgenomic era, DNA sequences with billions of informational elements are currently accumulating in the data banks. Consequently, the need of translating the linear information of the base sequences into functional elements is becoming more and more crucial.

In a recent past, the DNA chain was considered to be substantially homogeneous in its canonical structure and acting as a simple repository of the genic information. This homogeneity appeared to hinder reading the information encoded in the base sequence. Therefore, DNA expression

* Corresponding author. Tel.: +39 06 4991 3228; fax: +39 06 445 3827.
E-mail address: pasquale.desantis@uniromal.it (P. DeSantis).
[1] Present address: SISSA/ISAS, Via Beirut 4, I-34014 Trieste, Italy.

0301-4622/$ - see front matter © 2004 Elsevier B.V. All rights reserved.
doi:10.1016/j.bpc.2004.09.007

and control were supposed to be fully delegated to proteins.

On the contrary, DNA is now being recognised more and more extensively as a complex polymorphic macromolecule, which plays a relevant part in the management of the gene information it contains.

In fact, the present concept of gene includes the control regions preceding and following the coding region as well as the introns. Moreover, the intergenic regions could have a role in driving, e.g., in eukaryotic genomes, the complex architecture of chromatin as well as other structural and regulative functions.

Every function of DNA, including transcription, replication and recombination, is guided by deviations from the monotonous regularity of the straight canonical B-DNA structure and dynamics. Such structural deviations are an intrinsic property of the sequence and are recognized and amplified by protein binding. This requires a free-energy balance that is paid by the protein interactions, but minimized by suitable intrinsic structural properties of the DNA tract involved in the recognition. This is particularly evident in the case of sequence-dependent DNA-histone octamer association, the nucleosome, which governs the packaging and the superstructural organization of the genome as well as the gene regulation [1].

In conclusion, an important part of the DNA information content is not localized on the codogenic regions but appears to be related to the nanoscale DNA mechanical properties.

Several authors have focused their attention to the static and dynamic superstructural effects produced by the local distortions from the canonical B-DNA structure.

Historically, the first hypothesis about bent DNAs was proposed as the cause of the aberrant electrophoretic behaviour of some DNA sequences in the 1970s [2–4]. Analyzing the nucleotide sequence of eukaryotic DNAs, Trifonov and Sussman [5] found a weak periodicity of some dinucleotide steps along the sequence with a period close to the DNA helical repeat. They suggested that the angles between base-pair planes (the "wedge angle") are sequence dependent and that the observed periodicity reflects the anisotropic flexibility of the DNA molecule. As Trifonov and Sussman pointed out, even small structure variations (for example, due to wedge angles) could have a considerable influence on the global DNA bendability when they are phased with the DNA helical turn.

Two years later, Marini et al. [6] advanced the concept of the static bend as a sequence-dependent DNA property, as a result of their investigations on the electrophoretic anomalies of a Kinetoplast DNA tract of *Leishmania tarentolae*. Afterwards, Wu and Crothers [7] localized the bend in that DNA tract introducing the electrophoresis gel permutation assay. It consists in localizing the minimum of the retardation plot of cyclically permuted DNA tracts, obtained by single restrictions on the tandem dimer of the tract considered.

Systematic investigations about the origin of DNA curvature were carried out by Hagerman [8] and Koo et al. [9] using the anomalies of polyacrylamide gel electrophoresis, quantified by the retardation factors, the ratio between the apparent and actual bp numbers, associated to biosynthetic multimeric oligomers. Crothers et al. advanced the hypothesis that deviations from linearity should occur at the boundary between the normal B-DNA structure and AA·TT repeating stretches longer than three base pairs.

Later, several authors proposed models to describe the curvature in terms of the dinucleotide unit structure. The wedge angle between consecutive base pairs is assumed to be different for each dinucleotide step. Wedge angles in phase with the helix periodicity can produce an effective curvature, which could be large enough to be macroscopically detected. These models generally assume that the wedge angles are only dependent upon nearest-neighbour interactions and they are therefore called nearest-neighbour models [10–14]. They were recently reviewed by Crothers [15], who verified their effectiveness in predicting intrinsic DNA curvature in good agreement with the experiments. One of these models has been developed by our group [10,11] and will be described in more details in the next sections.

In addition, Olson et al. [14] have performed a systematic analysis of the dispersion of base-pair parameters in DNA crystal structure to have an estimate, in the framework of first-order elasticity, of the dinucleotide sequence-dependent deformability, as well as the correlation between fluctuations of different parameters. Indeed, all dinucleotide steps show concerted variations of roll, tilt, twist, shift and slide parameters, probably in order to relieve the close steric contacts between bases, whereas the rise varies almost independently of all the other parameters [14].

More recently, we proposed a set of dinucleotide rigidity parameters, expressed in terms of the normalized melting temperatures, as a measure of the DNA differential flexibility along the sequence. These parameters can predict free energies of competitive nucleosome reconstitution experiments in good agreement with the experimental results [16,17].

Moreover, since the first evidence of DNA anomalous electrophoretic mobility, large amounts of other experimental data have shown that many DNAs are curved or exhibit tracts with preferential bendability. Many different experimental methods have been used to this aim, such as light scattering [18,19], ligase-catalyzed cyclizations [20], flow dichroism [21], transient electric birefringence [22,23] and transient electric dichroism [24,25]. However, all these methods need simplifying models to interpret the data, which can affect the results.

On the contrary, progress in the direct visualization of macromolecules allows the analysis of morphological properties and structural changes of DNAs directly from the digitised micrographs of single molecules (Fig. 1).

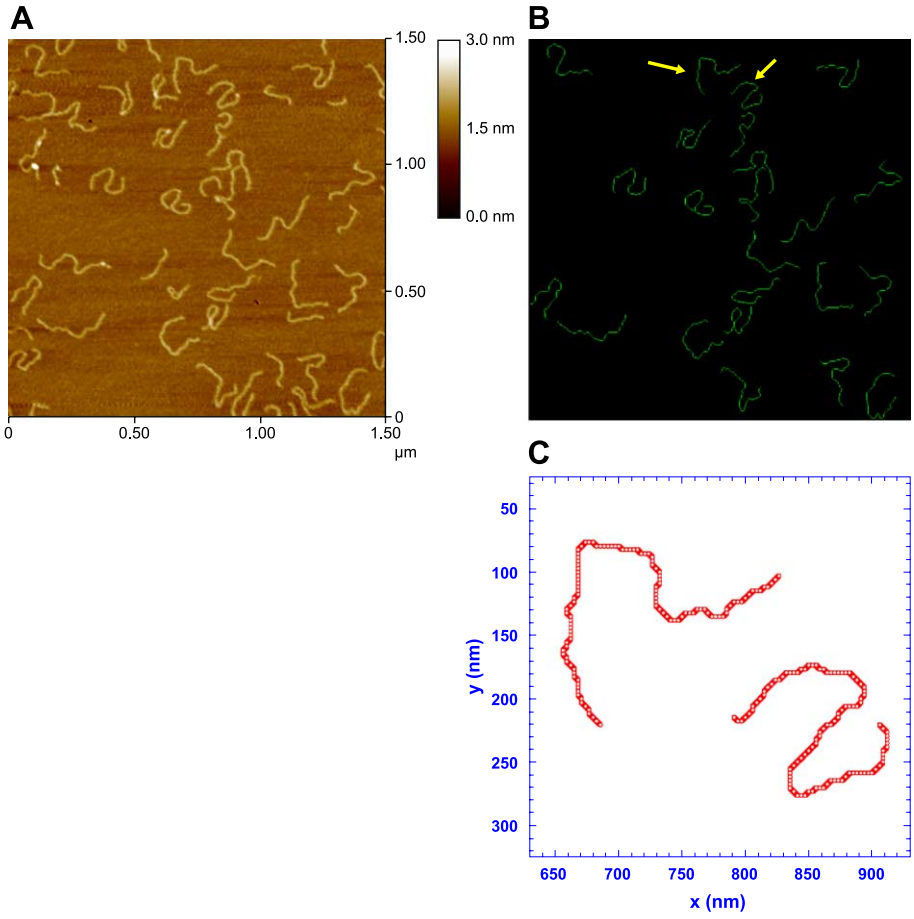

Fig. 1. (A) Example of SFM images of intrinsically bent DNA molecules. (B) The same molecules in panel (A) after digitalization. When it was not possible to extrapolate the correct 2-D path, such as for incomplete, fragmented or superimposed molecules, the images were skipped. Panel (C) report as example the magnification of the two molecules in panel (B), indicated by the arrows (images and data are a courtesy of Sabrina Pisano).

The statistical analysis of a large number of molecules, in order to get more reliable results, could bring information both on the local intrinsic curvature and the flexibility of DNA tracts at nanometric scale in relatively long sequences.

The next section will describe the various methodologies proposed by different authors.

Alternatively, for a more specific discussion about manipulation of single molecules and DNA mechanics under stretching by external forces, we refer to other recent reviews [26–29].

2. The worm-like chain model

The classical theory for describing DNA conformations at nanometric scale is the worm-like chain model (WLC), initially proposed by Kratky and Porod [30] and later revisited by various authors [31–34]. In this model, the stiffness of the chain is represented by its persistence length (P), which can be interpreted either as the projection of the whole polymer chain onto its starting direction or the distance over which the memory of an initial orientation of the polymer persists. It is the correlation integral between the direction of pairs of tangent unit vectors, $\mathbf{u}(s)$ and $\mathbf{u}(s')$, to the profile of the curved DNA tract separated by the curvilinear distance l:

$$\langle \mathbf{u}(s)\mathbf{u}(s') \rangle = \exp(-l/P) \quad (1)$$

A limitation of the initial WLC model was the assumption of intrinsically straight homogeneous polymers whose thermal fluctuations are quantified as deviations from the straight line. However, DNA almost always contains curved regions, which can strongly affect the persistence length. The intrinsic bent regions contribute to the experimentally measured persistence length (P_a) with a term denoted as the static persistence length (P_s), whereas thermal fluctuations contribute with the dynamic persistence lengths (P_d). The three contributions are related by

$$1/P_a = 1/P_d + 1/P_s \quad (2)$$

as initially proposed by Trifonov et al. [35] and later checked by Schellman and Harvey [36]. Such relation

can be obtained as the sum of the angular dispersions of the unit vectors along the curvilinear DNA profile due to both the static curvature and dynamic fluctuations under the hypothesis of their mutual independence [37].

As aforementioned, scanning force microscopy (SFM), electron microscopy (EM) and cryoelectron microscopy, where molecules are absorbed onto supporting films, have the advantage of directly observing the DNA path. However, the preparation of specimens exposes DNA to strong perturbations, which can introduce artefacts in the measurements of the persistence length. First of all, during adsorption, DNA molecules are transformed from a three-dimensional (3-D) into a two-dimensional (2-D) object. EM techniques need the drying and staining of the samples. In addition, the finite size of the tip used in SFM experiments and the image processing make difficult to determine high-curvature features within the range of the experimental resolution.

As regards the first point, two extreme cases can be described [38]: the molecules freely equilibrate on the surface, before being trapped in a particular conformation, or the molecules adhere without having equilibrated on the substrate, resembling the actual 3-D conformations. In the latter case, the conformations of the molecules reflect the history of their approach to the surface and it is therefore difficult to distinguish between intrinsic conformations and those induced upon adsorption. However, Bednar et al. [39] pointed out that cryoelectron microscopy experiments need no adsorption of the molecules on a surface and, contrary to classical EM, need no staining or drying of the samples. Molecules are suspended in a thin layer of a cryo-vitrified buffer. Although this confinement can cause some changes in the preferred DNA shapes, the high speed of cooling leaves only few possibilities to DNA to change its conformations. In addition, the actual 3-D DNA structures can be reconstructed from the combined use of two stereo micrographs [39].

In the case of the molecules that freely equilibrate on the surface, it is possible to have an ensemble of 2-D conformations, which can be related to the actual 3-D DNA structures, as will be described in the next section.

3. DNA persistence length in two dimensions

Given a polymer chain with a persistence length, P, in the framework of first-order elasticity, the energy required to bend by an angle θ, two segments located at a certain distance l, is [40]:

$$E = \frac{RTP}{2l}\theta^2 = \frac{1}{2}b\theta^2 \tag{3}$$

where R is the ideal gas constant and T is the absolute temperature, whereas $b=RTP/l$ is the apparent bending force constant. Therefore, in two dimensions, the probability of having a certain bend angle follows a Gaussian distribution

$$p(\theta)_{2D} = \sqrt{\frac{P}{2\pi l}}\exp\left(-\frac{P}{2l}\theta^2\right) \tag{4}$$

The hypothesis of Gaussian distribution is generally considered sound. To test if the molecules ensemble is statistically valid, some authors [38,41] have proposed the measurement of the ratio $\langle\theta^4\rangle_{2D}/\langle\theta^2\rangle^2_{2D}$ or $\langle\theta^6\rangle_{2D}/\langle\theta^2\rangle^3_{2D}$, which should be equal to 3 and 15, respectively, for Gaussian distributions. The values found by Frontali et al. [41] in EM experiments and Rivetti et al. [38] in SFM experiments were generally very close to the expected values, even if Rivetti et al. found some deviations for very short l, probably due to the SFM limit resolution, and for l close to the DNA contour length.

Following Eq. (4), Rivetti et al. obtained the average cosine of the angle between segments separated by a distance, l, as a function of the persistence length, P:

$$\langle\cos(\theta)\rangle_{2D} = \int_{-\infty}^{\infty} p(\theta)_{2D}\cos(\theta)\mathrm{d}\theta = \exp\left(-\frac{1}{2P}\right) \tag{5}$$

Eq. (5) was therefore used to calculate the mean square end-to-end distance of the polymer:

$$\begin{aligned}\langle R^2\rangle_{2D} &= \int_0^L\int_0^L \langle\mathbf{u}(s)\mathbf{u}(s')\rangle\mathrm{d}s\mathrm{d}s' \\ &= \int_0^L\int_0^L \langle\cos(\theta)\rangle\mathrm{d}s\mathrm{d}s'\end{aligned} \tag{6}$$

where $\mathbf{u}(s)$ and $\mathbf{u}(s')$ are the unit tangent to the chain at the positions s and s' respectively, and L is the DNA contour length. Resolving Eq. (6) gives

$$\langle R^2\rangle_{2D} = 4PL\left(1-\frac{2P}{L}\left(1-\exp\left(-\frac{L}{2P}\right)\right)\right) \tag{7}$$

Following Kratky and Porod [30], in three dimensions, the mean square end-to-end distance of the polymer is:

$$\langle R^2\rangle_{3D} = 2PL\left(1-\frac{P}{L}\left(1-\exp\left(-\frac{L}{P}\right)\right)\right) \tag{8}$$

This means that a molecule, which freely equilibrates on the surface, has an apparent persistence length, which is twice than that found for the 3-D structure. On the contrary, projecting a 3-D state onto a flat surface, results in having a mean square end-to-end distance equal to 2/3 $\langle R^2\rangle_{3D}$.

Rivetti et al. [38] proposed the differences between $\langle R^2\rangle$ values to be able to discriminate between molecules that have equilibrated on the surface from those which have not. The authors found that some molecules deposited on glow-discarded mica or water-treated mica have $\langle R^2\rangle$ values very close to the expected values for trapped molecules; on the

other hand, molecules deposited onto untreated freshly cleaved mica were able to equilibrate on the surface. They found that the DNA persistence length was 52 nm, in good agreement with the data found with other techniques.

Another reason that in principle could affect the measured persistence length is the excluded volume effects, which can increase the measured rigidity of the chains [38]. However, Monte Carlo simulations showed that these effects could be neglected for contour lengths shorter than 1000 nm (~20 persistence lengths).

Eqs. (4)–(8) can be used to obtain a number of statistically relevant parameters for intrinsically straight DNAs.

However, DNA almost always contains curved regions or tracts with different flexibility, depending on the sequence, which can strongly affects the persistence length. It was therefore necessary to extend the WLC model to these cases.

The first attempt was proposed by Muzard et al. [42]. Assuming a static angle between two segments along a chain, reflecting the local curvature, the cosine of the angle between the two segments at a certain curvilinear distance, s, is

$$\langle \cos(\theta) \rangle = \exp(-s/P)\cos(\kappa s) \tag{9}$$

where κ is the inverse of the local radius of curvature of the chain (assuming that curvature does not vary within small regions of the molecule).

In two dimensions, given a certain DNA tract, the local curvature can be simply characterized by the ratio, SD, of the curvilinear distance to the linear end-to-end distance of the tract (Fig. 2A). Therefore, SD is close to 1 for straight chains and is higher than 1 for curved regions. It should be noted that SD actually corresponds to $(\theta/2)/\sin(\theta/2)$, which converges to $1+\theta^2/4!$ for real DNA chains (when θ is expressed in radians).

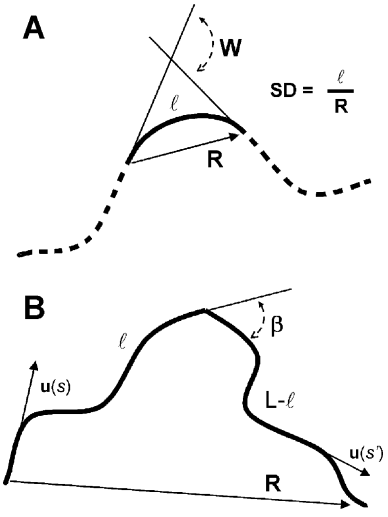

Fig. 2. (A) Schematic representation of a DNA tract characterized by the ratio, SD, of the curvilinear distance, ℓ, to the linear end-to-end distance of the tract, R. W is the wedge angle between the tangent vectors at both the ends of the DNA tract. (B) Schematic representation of a polymer chain, with a contour length L, including a static bend, β, at a certain position ℓ. R represents the end-to-end distance, whereas $\mathbf{u}(s)$ and $\mathbf{u}(s')$ are the tangents to the chain at the positions s and s', respectively. (Adapted from Ref. [46]).

Given θ, (w in the original paper) the experimental mean dinucleotide wedge angle for an N-bp DNA tract, $\theta=W/N$, where W is the wedge angle between the tangent vectors at both the ends of the DNA tract. θ is inversely proportional to the mean radius of curvature ($\theta/\kappa=s/N$) and can be directly deduced from the experimental value of SD [42]. Therefore, measuring SD for different DNA tracts along the chain eventually results in an estimate of the local curvature. The authors produced by EM several images of linearized pBR322 DNA molecules, obtained by different restriction enzymes and labelled by streptavidin–ferritin–biotin complex [43]. Secondly, they proceeded to evaluate the map of both the wedge curvature (θ) and the parameter kappa (κ) along the DNA chains. The authors underlined how curvature maps, when superimposed two at a time, showed many similarities in valleys and peaks, proving that, despite dynamic fluctuations of the single molecules and the deformations effects, due to the adsorption on a 2-D surface, the intrinsic features of the DNA sequence were largely conserved. Similar results were found for the κ maps, although they showed lower sensibility.

Finally, the authors compared the experimental average curvature maps with the results from four different theoretical models [9,10,44,45]. They found all the theoretical sets of data show very comparable features, correctly predicting the principal curved regions along the pBR322 tracts.

Rivetti et al. [46] proposed a quite different approach. Eq. (1) is valid for every couple of segments along a chain, independently of the distance $l=s-s'$. Therefore, in three dimensions, considering a static bend, β, located at a certain distance, ℓ, from one end of a polymer (Fig. 2B), it is possible to write:

$$\begin{aligned}\langle \mathbf{u}(s)\mathbf{u}(s') \rangle &= \langle \mathbf{u}(s)\mathbf{u}(\ell)\cos\ \beta \langle \mathbf{u}(\ell)\mathbf{u}(s') \rangle \\ &= \cos\ \beta\ \exp(-l/P)\end{aligned} \tag{10}$$

which is practically equivalent to Eq. (9). Eq. (10) is independent of the location of the bend angle between the position s and s' and could be used for a generalization of Eq. (7). In fact, Eq. (6) becomes

$$\begin{aligned}\langle R_\beta^2 \rangle_{2D} = &\int_0^\ell \int_0^\ell \langle \mathbf{u}(s) - \mathbf{u}(s') \rangle \mathrm{d}s\mathrm{d}s' \\ &+ 2\int_0^\ell \int_\ell^L \langle \mathbf{u}(s) - \mathbf{u}(s') \rangle \mathrm{d}s\mathrm{d}s' \\ &+ \int_\ell^L \int_\ell^L \langle \cos(\mathbf{u}(s) - \mathbf{u}(s')) \rangle \mathrm{d}s\mathrm{d}s'\end{aligned} \tag{11}$$

The first and third terms are practically equivalent to Eq. (6). The second term can be integrated introducing Eq. (10). Therefore,

$$\langle R_\beta^2\rangle = 2PL\left\{1-\frac{P}{L}\left[\left(1-\exp\left(-\frac{\ell}{P}\right)\right)+\left(1-\exp\left(-\frac{L-\ell}{P}\right)\right)+-\cos\beta\left(1-\exp\left(-\frac{\ell}{2P}\right)\right)\times\left(1-\exp\left(-\frac{L-\ell}{2P}\right)\right)\right]\right\} \quad (12)$$

which could be approximated, when both ℓ and $L-\ell$ are greater than $2P$, to

$$\langle R_\beta^2\rangle \approx 2PL\left(1-\frac{P}{L}(2-\cos\beta)\right) \quad (13)$$

In general, real DNA chains possess more than one bend, and several tracts with different flexibility, depending on the sequence. Eq. (12) can be extended to the case when N coplanar bends are present, separated by $N+1$ polymer sections of length ℓ_n, with different flexibility. The final formulation is quite complex [46]

$$\begin{aligned}\langle R^2_{\beta_1\ldots\beta_N,P_1\ldots P_{N+1}}\rangle_{2D} = 2\Bigg\{&\sum_{n=1}^{N+1}P_n\ell_n\left[1-\frac{P_n}{\ell_n}\left[\sum_n\times\left(1-\exp\left(-\frac{\ell_n}{P_n}\right)\right)\right]\right.\\&+\sum_{n=1}^{N}P_nP_{n+1}\cos\beta_n\times\left(1-\exp\left(-\frac{\ell_{n+1}}{P_{n+1}}\right)\right)\times\left(1-\exp\left(-\frac{\ell_n}{P_n}\right)\right)\\&+\sum_{n=1}^{N-1}\sum_{m=n+2}^{N+1}P_nP_m\cos\left(\sum_{i=n}^{m-1}\beta_i\right)\times\left(\prod_{j=n+1}^{m-1}\exp\left(-\frac{\ell_j}{P_j}\right)\right)\times\left(1-\exp\left(-\frac{\ell_n}{P_n}\right)\right)\times\left(1-\exp\left(-\frac{\ell_m}{P_m}\right)\right)\end{aligned} \quad (14)$$

Eqs. (12)–(14) are valid in three dimensions, but could be easily extended in two dimensions by multiplying the persistence length values by a factor 2. The authors tested Eq. (14) by using SFM imaging DNA fragments containing from two to eight phased A-tracts; this corresponds to introducing an increasing bent angle in the DNA molecules.

Analogously, to test Eq. (14) for tracts with different flexibility, Rivetti et al. [46] studied DNA fragments with single-stranded region with different lengths by SFM. Also in this case, the fitting of the mean square end-to-end distance was quite good, at least for short gap sizes, leading to the value of 1.3 nm for the single-stranded DNA.

More recently, Cognet et al. [47] proposed a different method to quantify the average values of the intrinsic bends and the local flexibility from SFM images. When a static bend is present, Eq. (4) assumes a slightly different formulation:

$$p(\theta) = \sqrt{\frac{P}{2\pi l}}\exp\left(-\frac{P}{2l}(\theta-\langle\theta\rangle)^2\right) \quad (15)$$

Therefore, in the framework of first-order elasticity, the bend angle, θ, is distributed around the mean value, $\langle\theta\rangle$, with a standard deviation $\sigma=(l/P)^{1/2}$. Considering the DNA profile as a chain of rods with the same length m forming angles, the total angle standard deviation can be expressed as

$$\sigma^2 = \left(\frac{2m}{3}+\frac{1}{3m}\right)\sigma_0^2 \quad (16)$$

where σ_0^2 is the standard deviation of the bend angles at the junction of the two DNA tracts [47].

As the authors considered only three points each time on the DNA molecules, if the segments are short enough, the standard deviation of the angle formed by the three points follows Eq. (16). Analysis of simulated EM images of 139-bp and 300-bp DNA molecules, as well as real EM images of 139-bp DNA molecules, showed that the values of σ^2 were in satisfactorily agreement with Eq. (16), if DNA tracts shorter than 70 bp were considered. Some deviations were also found in the case of real DNAs for tracts shorter than 20 bp.

A different and general model for DNA in three and two dimensions was recently introduced [48–51], on the basis of the statistical thermodynamics of the canonical ensemble of the WLC model, characterized by continuous variations of the dynamic and static curvature along the DNA sequence. The model is capable of deriving the curvature and flexibility profile along the DNA sequence from SFM or EM images, as well as discriminating the static and dynamic contributions to the persistence length at a nanometric scale. In addition, within the limit of the ergodic hypothesis, the model consistently explains the slow dynamics of DNA single molecules in their 2-D thermal fluctuations on crystal surfaces. This model will be extensively described in the next paragraph.

4. Sequence-dependent persistence length

In previous works [48–51], we proposed a method to compare the DNA intrinsic curvature and local flexibility, measured by SFM, to the corresponding values evaluated by our theoretical model [16,17,49].

According to the classical formulation by Landau and Lifshitz [40], the curvature of a space line is more correctly defined as the derivative $C=\mathrm{d}\mathbf{u}/\mathrm{d}l$ of the tangent unit vector, $\mathbf{u}$, along the line, l. Its modulus is the inverse of the curvature radius and its direction is that of the main normal to the curve. In the case of DNA, the line corresponds to the helical axis and the curvature is a vectorial function of the sequence. It represents the angular deviation between the local helical axes of the nth and (n+1)th helix turns centred on the nth and (n+1)th dinucleotide step, respectively.

The DNA curvature is a sequence-dependent superstructural property, which is continuously changed by the thermal energy of environment. Assuming first-order elasticity corresponding to a linear response of the DNA to such energy exchanges, the ensemble average value of the curvature is:

$$\langle \mathbf{C}(n)\rangle = \langle \mathbf{C}_0(n) + \chi(n)\rangle = \mathbf{C}_0(n) + \langle \chi(n,t)\rangle \tag{17}$$

where $\mathbf{C}(n)$ is the curvature at nth position, $\mathbf{C}_0(n)$ is the corresponding intrinsic curvature, and $\boldsymbol{\chi}(n,t)$ represents the dynamic fluctuation at a certain time, t. The latter term in Eq. (17), which corresponds to the dynamic contribution to the curvature, is obviously zero. Therefore, the intrinsic curvature, $\mathbf{C}_0(n)$, is the statistical average of the curvature at the nth sequence position or alternatively, the time average of the DNA superstructure.

Therefore, in the framework of the first-order elasticity, the curvature is distributed around the average intrinsic curvature, $\mathbf{C}_0(n)$, with a standard deviation $\sigma(\mathbf{C}(n))=\langle \boldsymbol{\chi}^2(n)\rangle^{1/2}$.

As a consequence, assuming a statistical thermodynamic canonical ensemble, the curvature dispersion at the nth position becomes

$$\langle \chi^2(n)\rangle = \frac{1}{Q(n)}\int \chi^2(n)\exp\left(-\frac{b(n)}{2RT}\chi^2(n)\right)d\chi(n) = \frac{RT}{b(n)} \tag{18}$$

where $b(n)$ represents the apparent bending force constant per bp at the nth position and where

$$Q(n) = \int \exp\left(-\frac{b(n)}{2RT}\chi^2(n)\right)\mathrm{d}\chi(n) \tag{19}$$

where the curvature dispersion is obtained by integrating Eqs. (18) and (19) in the complex plane [49]. The result of Eq. (18) is well known in solution [34].

However, when DNA is forced on a 2-D surface, the curvature becomes a real quantity and the phase information is reduced to the sign of the curvature. In this case, due to SFM resolution limits, a DNA molecule should be represented as a segmental chain of nanometric virtual bonds. Therefore, SFM or EM experiments permit to measure the curvature corresponding to the angle between the m-bp virtual segments at the nth sequence position, $C_m(n)$, as well as the corresponding dynamic contribution, $\chi_m(n)$. The segmental curvature, $C_m(n)$, is however half of the curvature $C(n,2m)$, which represents the angular deviation of the local helical axes of two nucleotide steps separated by $2m$ bp (Fig. 3). The latter term can be calculated from the theoretical intrinsic DNA curvature [52,53]:

$$C(n,2m) = \pm\left|\sum_{n-m}^{n+m} s\mathbf{C}_0(s)\right| \tag{20}$$

where the sign is chosen negative or positive if curvature produces clockwise or counterclockwise rotations of the segments along the chain, with respect to the average plane of the curved tracts [48–50].

Therefore, the $2m$-bp squared curvature deviation, $\chi^2(n,2m) = |\mathbf{C}(n,2m)-\mathbf{C}_0(n)|^2$, on average is

$$\langle \chi^2(n,2m)\rangle = \frac{1}{Q(n,2m)}\int_{-\infty}^{\infty}\chi^2(n,2m)\exp \times\left(-\frac{b(n)}{4mRT}\chi^2(n,2m)\right)\mathrm{d}\chi(n,2m) = \frac{2mRT}{b(n)} \tag{21}$$

where

$$Q(n,2m) = \int_{-\infty}^{\infty}\exp\left(-\frac{b(n)}{4mRT}\chi^2(n,2m)\right)\mathrm{d}\chi(n,2m) \tag{22}$$

The experimentally measured $\chi_m^2(n)$ is $\chi^2(n,2m)/4$, since dependent on the curvature thermal fluctuations of $2m$ bp.

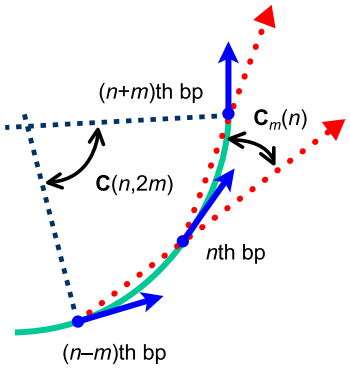

Fig. 3. Schematic representation of the segmental curvature, $C_m(n)$, at the nth sequence position. It corresponds to the angle between the two virtual segments linking the ($n-m$)th nucleotide step with the nth, and the nth nucleotide step with the ($n+m$)th, respectively. $C_m(n)$ is half of the curvature $C(n,2m)$, which represents the angular deviation of the local helical axes pertinent to nucleotide steps separated by $2m$ bp. (Adapted from Ref. [50]).

Its square root corresponds to the standard deviation of $C_m(n)$ around its mean, $\sigma(C_m(n))=[mRT/(2b(n))]^{1/2}$. Therefore, it only depends on the differential flexibility along DNA sequence, expressed by $b(n)$.

On the contrary, as aforementioned, some authors [38,39,42,46,47] used approximate evaluation of the curvature as related to the ratio between the chain contour length and the corresponding cord, which, actually, corresponds to $\theta/2\sin(\theta/2)$ for real DNA chains. Nevertheless, in the investigated cases, an apparent qualitative agreement was found with the theoretical predictions of DNA intrinsic curvature [42].

However, the average curvature modulus, $\langle|C_m(n)|\rangle$, contains both the static and the dynamic curvature contributions, i.e., it is related to both the intrinsic curvature and the curvature fluctuations involving $2m$ bp.

As a suitable approximation for curvatures of interest, the following compact formulation is obtained for $\langle|C_m(n)|\rangle$ [49,50]:

$$\langle|C_m(n)|\rangle = \frac{\langle|C(n,2m)|\rangle}{2} = \left[\frac{2}{\pi}\left(\langle C_m(n)\rangle^2 + \frac{mRT}{2b(n)}\right)\right]^{\frac{1}{2}} \tag{23}$$

This result clearly points out that the average curvature modulus depends on two terms: one is the intrinsic curvature and the other represents the sequence-dependent flexibility of the chain. The standard deviation of curvature modulus is [49,50]

$$\sigma(|C_m(n)|) = \left[\left(\frac{\pi-2}{\pi}\right)\left(\langle C_m(n)\rangle^2 + \frac{mRT}{2b(n)}\right)\right]^{\frac{1}{2}} \tag{24}$$

Unexpectedly, both the average curvature modulus and the relative standard deviation have the same dependence on the intrinsic curvature and flexibility. They are proportional and their ratio is $[2/(\pi-2)]^{1/2}$, contrary to the general feeling that associates the flexibility to the curvature modulus dispersions. Such a concept is correct only when the curvature phases are taken into account.

5. Mapping DNA curvature and flexibility from SFM images

In recent papers, we showed the profiles of the average curvature modulus and the corresponding standard deviation along the chain obtained from the SFM images of the 1878-bp dimer of the *Eco*RV/*Pst*I fragment of *p*BR322 DNA [49] and of the 898-bp *Pvu*II fragment and 1010-bp *Nhe*I fragment from the plasmid *p*PK201/CAT [51]. The distribution of the pixel file, which interpolates the DNA chain, was normalized via Fourier transform operations. These convert the nonuniform pixel sequence of the DNA images in a uniform coordinate distribution along the contour length. After this transformation, the number of points, which interpolate the DNA traces, remains practically invariant and corresponds to the average value of pixels per molecule.

The profiles of the curvature modulus and the relative standard deviation show very similar trends, and a nearly constant ratio close to the theoretical value, in good agreement with Eqs. (23) and (24) (Fig. 4).

Furthermore, as this result was obtained assuming the canonical ensemble distribution, the existence of a strict relation between the average curvature modulus and the related standard deviation corresponds to fulfilling the condition of local thermodynamic equilibrium of the DNA tracts on 2-D surfaces.

An evaluation of $\langle b(n)\rangle$ led to the value of 85 kcal/bp rad^{-2}, corresponding to a rather standard persistence length of 48 nm in the 3-D state.

A satisfactory agreement was found between the experimental data of the average curvature modulus and their standard deviation along the chain and their theoretical values, adopting for $b(n)$ the average value of 85 kcal/bp rad^{-2}, supporting the hypothesis that the statistically averaged curvature modulus is a quantity dependent on the intrinsic DNA curvature and flexibility and does not allow the separation of the two contributions. Only in the case of an intrinsically straight DNA, when the intrinsic curvature vanishes, the standard deviation of the curvature modulus represents the differential flexibility along the sequence. Otherwise, the differential flexibility could be obtained only if the curvature with its relative phases is taken into account. Therefore, the persistence length obtained from measurements of end-to-end distance represents the average DNA stiffness only for intrinsically straight sequences; otherwise, it is affected by the effects connected to the intrinsic curvature integrated over the whole DNA tract considered.

Moreover, some authors [41,54] pointed out that the limit resolution implicit in the EM and SFM techniques makes it difficult to determine high-curvature features within the range of the experimental resolution and could affect the

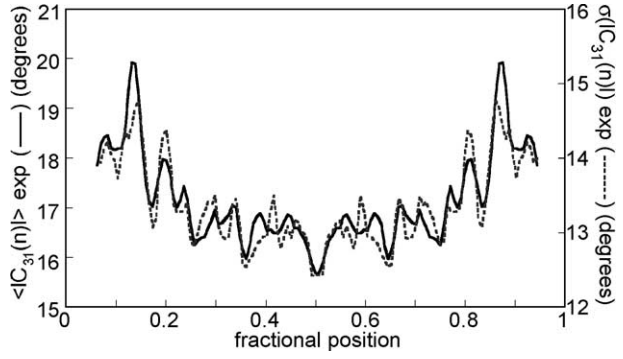

Fig. 4. Comparison between the profiles of the experimental average curvature modulus and the corresponding standard deviation along the DNA chains of the dimer of the *Eco*RV/*Pst*I *p*BR322 fragment (m=31 bp). (Adapted from Ref. [49]).

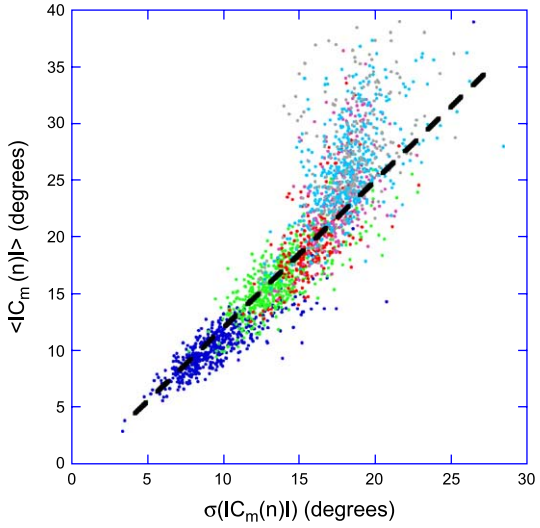

Fig. 5. Time-averaged curvature modulus, $|C_m(n)|$, and the relative standard deviation, $\sigma(|C_m(n)|)$, for different DNA segment lengths, m, averaged for the two linearized pBR322 molecules of Ref. [50] (blue: m=17; green: m=34; red: m=51; purple: m=68; cyan: m=85; gray: m=102). As shown in the figure, the values ratio taken at regular intervals along the sequence monitor the ergodicity of the DNA dynamics. When the length, m, of the considered DNA segments increases, the ratios deviate from the theoretical value of $(2/(\pi-2))^{1/2}$, and their dispersion increases as well. (Adapted from Ref. [50]).

persistence length measured by the local curvature analysis. This limit is both due to the finite size of the tip in SFM experiments and to the processing of the images to track the DNA path on the surface. van Noort et al. generated an ensemble of simulated SFM images of DNA molecules with different flexibility. They found the measured persistence length was overestimated with respect to that obtained from the end-to-end distance. However, the authors did not take into account the intrinsic flexibility of the adopted segmental chain for DNA images, as already discussed in the previous paragraph.

The ergodic theory allows the extension of Eqs. (23) and (24) to the time averages. Conversely, the experimental validation of these equations can be assumed as a proof of the thermodynamic reversibility of the local motions of DNA, because they were obtained adopting the canonical distribution.

We monitored the slow dynamics of two differently linearized pBR322 molecules by time-resolved SFM [50]. DNA curvature, considered with its modulus and direction on the mica surface, permitted the determination of its static and dynamic contributions. Therefore, the obtained sequence-dependent DNA static curvature and flexibility were in satisfactory agreement with the predictions. The large-scale dynamics of the two DNA molecules appeared to be far from the equilibrium and retained memory of the starting structure for hours. On the contrary, the local dynamics well represented the equilibrium time fluctuations, according to the principle of microscopic reversibility (Fig. 5).

6. Comparison between theoretical and experimental DNA curvature and flexibility

It is worth noting that the experimental resolution limits the quality of the information one can obtain from microscopy images, as it is necessarily an average of the local features over a distance characteristic of the resolution.

As an example, Fig. 6A reports the experimental profile of the curvature standard deviation along the chain for a 898-bp palindromic *Pvu*II fragment from the plasmid pPK201/CAT [51], obtained for recurrent 21-bp DNA tracts from the SFM images.

The profile of the standard deviation of the curvature obtained by the SFM images correlates both with the profile of the normalized local "premelting" temperature, previously proposed as a measure of the DNA differential flexibility along the sequence [48,49], as well as with the normalized volumes of conformational space, proposed as representative of the dinucleotide deformability by Olson et al. [14], despite the fact that the two initial sets of data are poorly correlated.

This means that different sets of dinucleotide deformability parameters can reproduce the experimental data with

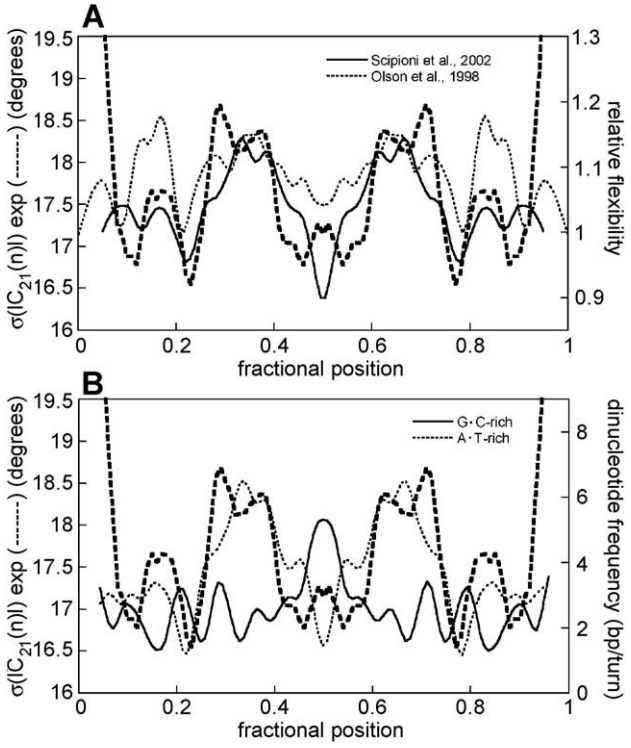

Fig. 6. (A) Comparison between the profiles of the experimental curvature standard deviation for a 898-bp palindromic *Pvu*II fragment from the plasmid pPK201/CAT [51] (m=21 bp) and the DNA differential flexibility, expressed as the normalized dinucleotide stacking energy [49] and as the normalized volumes of conformational space [14]. (B) Comparison between the experimental standard deviation of the curvature with the frequency of AT·AT+AA·TT+TA·TA (A·T-rich) and GC·GC+GG·CC+CG·CG (G·C-rich) dinucleotide steps along the DNA chain.

similar reliability when averaged over a significant number of base pair, in a way that is similar to that of the dinucleotide roll and tilt parameter sets proposed in the literature, which are scarcely correlated between each others, but which are nevertheless able to predict curvature in similar ways [10–15].

However, in general, the experimental standard deviation of the curvature seems to correlate better with the frequency of AT·AT+AA·TT+TA·TA dinucleotide steps along the DNA sequences than with the frequency of GC·GC+GG·CC+CG·CG dinucleotide steps (Fig. 6B). This suggests that the sequence determinants of the DNA flexibility are strictly correlated with those of DNA curvature; namely, the static and dynamic curvature are monotonous functions of the sequence.

7. Recognition effects by the crystal surface

As aforementioned, when scanning force microscopy (SFM) is used to obtain the sequence-dependent mechanical properties of DNA, molecules are absorbed onto crystal surfaces, which have the advantage of directly observing the DNA path molecules but transformed from a three-dimensional (3-D) into a two-dimensional (2-D) object. This could modify both the static and dynamic curvature. The experimental evidence shows that the latter effect can practically be explained by the reduction of degree of freedom in the chain dynamics with a consequent apparent doubling of bending force constant and related persistence length. Therefore, the thermal fluctuations seem to be influenced by the adsorption from crystal surfaces only for what they concern the time scales but not their amplitudes. However, the influence of the crystal surface on the static curvature is still an open problem. It depends on the ionic strength and the specific nature of cations as well as on the kind of pretreatments of crystal surface.

In recent investigations, dealing with this problem, indications of a preferential adsorption of one of the alternative prochiral faces of curved DNA tracts on the mica surface were reported [48,49].

Curved DNA gives rise to planar or quasi-planar superstructure, when the sequence is characterized by periodic recurrence of A-tracts phased with the B-DNA periodicity. It is worth noting that, when short AA·TT stretches are positioned on the same strand, the adenine bases tend to be preferentially oriented on one side of the curvature plane, while the complementary TT·AA stretches will be found on the other side. When deposited on a flat surface, these curved DNA tracts will therefore interact with the surface with either an A- or T-rich face (Fig. 7A and B).

To cast light on a possible recognition by the crystal surface, a highly curved DNA fragment from the kinetoplast DNA of *Crithidia fasciculata* [55] was recently investigated by analysing a large pool of SFM images deposited on the mica surface. However, to remove the uncertainty on the sequence orientation in the SFM images, the strategy of constructing palindromic DNA molecules was followed, as suggested in the literature [56].

The sequence of the two curved tracts in a palindromic construct is characterized by periodical recurrence of

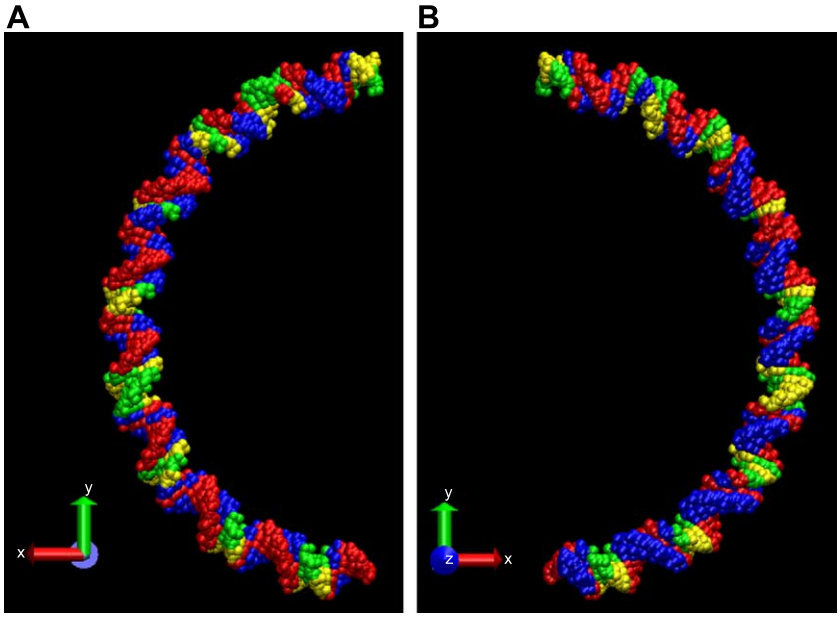

Fig. 7. (A and B) CPK representation of a curved DNA fragment from *C. fasciculata* [55]. The 3-D structure was generated by WebDNA program [53] Images were generated by means of VMD 1.8.2 program [78]. Red is for A, blue for T, green for G, and yellow for C. In panel (A), most of the thymines point toward the observer. If the structure is rotated by 180°, the bases are interchanged with those complementary. Therefore, in panel (B), the bases, which preferentially point toward the observer, are the thymines.

repeated AA·TT in the first tract followed by TT·AA steps in the other, and, conversely, TT·AA followed by AA·TT steps in the other palindromic construct. The intrinsic dyad symmetry is also reflected in the stereochemistry of the molecules but, in the 2-D case, only two alternative directions of the dyad axis are allowed, parallel or perpendicular to the surface plane. These symmetry species where called C- and S-like shapes, respectively (or C*- and S*-like shapes, the asterisk indicating the mirror image), because the curves are isomorphous with these letters.

These two possibilities are the result of the adhesion of the curved DNA tracts with either one of the two opposite A- or T-rich faces. As a result, C- and C*-shaped molecules expose equivalent faces to the surface. Instead, S- and S*-shaped molecules expose different faces (Fig. 8).

A large pool of SFM images were collected (about 1,500) of both head-to-head and tail-to-tail palindromic dimers of the *Crithidia* fragment. The measured average curvature profiles are interpreted as an evidence of the preferential binding of the surface with the T-rich face of the curved DNA tracts. In fact, for the tail-to-tail palindrome, the molecules with an S shape were five times as numerous as those in the S* class. Conversely, for the head-to-head dimer, the S* class is much more populated than the S class (nine times as much).

Such sequence-dependent differential interaction of curved DNAs with inorganic crystal surfaces was speculated to be implicated in prebiotic steps of DNA evolution [57] as well as to be useful in DNA-based nanotechnology.

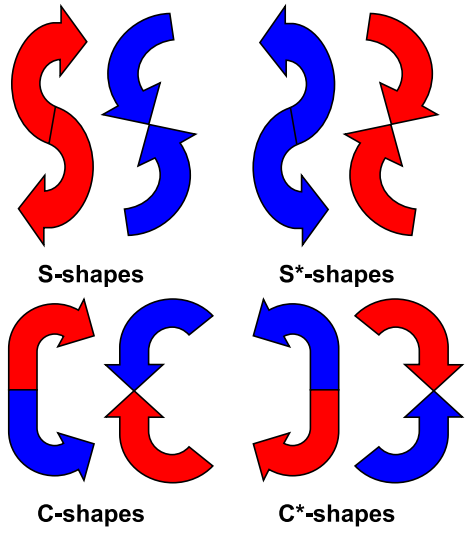

Fig. 8. Scheme of the tail-to-tail and head-to-head dimers on mica surface: S-shaped dimers in one case and S*-shaped dimers in the other expose the same faces to the surface. The C- and C*-shaped dimers expose both the types of faces (A- and T-rich) to the surface. (Adapted from Ref. [57]).

8. The effects of cationic metals on the persistence length

Several papers report that the fraction of bent molecules seen by EM or SFM was higher in the presence of cationic metals. This is not surprising, since it is known that Mg^{2+} can induce or enhance curvature in DNA fragments [58,59] and helps stabilize several types of DNA structures [60,61].

A few studies have shown that Mg^{2+} in the presence of uranyl acetate helps stabilize end-to-end interactions in cohesive ends DNA fragments [56,62]. In addition, divalent cations have been shown to favour right- to left-handed DNA transitions [63].

Frontali et al. [41] collected EM images of DNA fragments at different ionic forces (from 0.03 M to 0.5 M NH_4-acetate) showing that the measured persistence length varied from about 55 nm at high ionic force, to about 140 nm at lower ionic force. However, many papers have pointed out the effects of divalent cations on DNA curvature and flexibility, as these ions interact with DNA bases and phosphates. Laundon and Griffith [64] studied a 890-bp DNA containing the well-known *C. fasciculata* kinetoplast DNA fragment [55]. They found that the number of molecules that contained steep bend or loop in EM images was higher after treatment with metal ions. In particular, when the 890 bp was incubated in 10 nm Tris, pH 7.5, and 0.1 mM EDTA, the percentage of looped molecules was only 2–3%. On the contrary, when DNA molecules were incubated in the presence of cationic metals, the percentage of looped molecules increased up to 60% of the total. The type and the concentration of the ions were effective in inducing loops: Cu^{2+}, Co^{2+}, Ni^{2+} and Zn^{2+} ions were maximally effective at concentrations of 5–10 mM, Mn^{2+} and Ba^{2+} at 50–100 nM, and finally, Mg^{2+} and Ca^{2+} at 0.5–1.0 M. In general, the fraction of looped or highly bent molecules in the case of Mg^{2+} (or Ca^{2+}) was lower than that found for the other cations.

More recently, Zn^{2+} ions were shown to kink DNA at low concentrations. SFM images of 168-bp DNA circles in 1 mM Zn^{2+} appear very different from their counterparts in 1 mM Mg^{2+} [65]. In the first case, the authors observed 184 kinks in 204 molecules, whereas 621 kinks in 162 molecules were observed in Zn^{2+}, namely, an increase from 0.9 to 3.8 kinks per molecule. The authors underlined that the action of Zn^{2+} is not inhibited by increasing Mg^{2+} concentration, a result that is consistent with different binding sites for the two ions. However, they pointed out the activity of the ions could be different on the mica with respect to the solution.

9. DNA-based nanoarchitectures and nanomotors

The large progress of biotechnology, have recently provided the inspiration for the use of DNAs as building

blocks for increasing level of complexity of self-assembling architectures, in the recent explosive development of nanotechnology and nanoscience. The precise self-complementary strand recognition and the high variety of informational content associated to the sequence offer a wide panorama of perspectives for nanotechnological devices and nanomotors inspired by the biological mechanisms involving DNA. The complex 2-D and 3-D DNA molecular architectures based on the blocked Holliday junction, first designed and realised by Seeman [66], represent impressive examples of the high power of auto-assembly coded in the DNA sequence. In addition, such superstructures are sensitive to the environment and can undergo structural transitions under appropriate conditions acting as nanomachines, changing the distance of separation of object in space [67], or nanomotors, in response of cyclic environment changes. Other authors recently reported examples where different conformational transitions of DNA constructs have been exploited to move objects around. [68–77].

Acknowledgements

The authors would like to thank Maria Savino (Dept. of Genetics and Molecular Biology) and Bruno Samorì (Università di Bologna) for useful discussions.

CA would like to thank Sabrina Pisano (Dept. of Genetics and Molecular Biology) for providing SFM images of curved DNAs.

This work was supported by: “Progetto 60% Ateneo” of University “La Sapienza”, 2003 MIUR, Progetti di Ricerca di Interesse Nazionale 2004, and by Istituto Pasteur, Fondazione Cenci-Bolognetti.

References

[1] R.D. Kornberg, Structure of chromatin, Annu. Rev. Biochem. 46 (1977) 931–954.
[2] K. Danna, D. Nathans, Specific cleavage of simian virus 40 DNA by restriction endonuclease of *Hemophilus influenzae*, Proc. Natl. Acad. Sci. U. S. A. 68 (1971) 2913–2917.
[3] K. Danna, D. Nathans, Bidirectional replication of Simian Virus 40 DNA, Proc. Natl. Acad. Sci. U. S. A. 69 (1972) 3097–3100.
[4] J.E. Mertz, P. Berg, Viable deletion mutants of simian virus 40: selective isolation by means of a restriction endonuclease from *Hemophilus parainfluenzae*, Proc. Natl. Acad. Sci. U. S. A. 71 (1974) 4879–4883.
[5] E.N. Trifonov, J.L. Sussman, The pitch of chromatin DNA is reflected in its nucleotide sequence, Proc. Natl. Acad. Sci. U. S. A. 77 (1980) 3816–3820.
[6] J.C. Marini, S.D. Levene, D.M. Crothers, P.T. Englund, Bent helical structure in kinetoplast DNA, Proc. Natl. Acad. Sci. U. S. A. 79 (1982) 7664–7668.
[7] H.M. Wu, D.M. Crothers, The locus of sequence-directed and protein-induced DNA bending, Nature 308 (1984) 509–513.
[8] P.J. Hagerman, Sequence-directed curvature of DNA, Nature 321 (1986) 449–450.
[9] H.S. Koo, H.M. Wu, D.M. Crothers, DNA bending at adenine · thy- $thyminetracts, Nature320(1986)501 - -503$.
[10] P. De Santis, A. Palleschi, S. Morosetti, M. Savino, Structure and superstructures in periodical polynucleotides, in: E. Clementi, S. Chin (Eds.), Structures and Dynamics of Nucleic Acids, Proteins and Membranes, Plenum Press, New York, 1986, pp. 31–49.
[11] P. De Santis, A. Palleschi, M. Savino, A. Scipioni, Validity of the nearest-neighbor approximation in the evaluation of the electrophoretic manifestations of DNA curvature, Biochemistry 29 (1990) 9269–9273.
[12] A. Bolshoy, P. McNamara, R.E. Harrington, E.N. Trifonov, Curved DNA without A–A: experimental estimation of all 16 DNA wedge angles, Proc. Natl. Acad. Sci. U. S. A. 88 (1991) 2312–2316.
[13] A.A. Gorin, V.B. Zhurkin, W.K. Olson, B-DNA twisting correlates with base-pair morphology, J. Mol. Biol. 247 (1995) 34–48.
[14] W.K. Olson, A.A. Gorin, X.-J. Lu, L.M. Hock, V.B. Zhurkin, DNA sequence-dependent deformability deduced from protein–DNA crystal complexes, Proc. Natl. Acad. Sci. U. S. A. 95 (1998) 11163–11168.
[15] D.M. Crothers, DNA curvature and deformation in protein–DNA complexes: a step in the right direction, Proc. Natl. Acad. Sci. U. S. A. 95 (1998) 15163–15165.
[16] C. Anselmi, G. Bocchinfuso, P. De Santis, M. Savino, A. Scipioni, Dual role of DNA intrinsic curvature and flexibility in determining nucleosome stability, J. Mol. Biol. 286 (1999) 1293–1301.
[17] C. Anselmi, G. Bocchinfuso, P. De Santis, M. Savino, A. Scipioni, A theoretical model for the prediction of sequence-dependent nucleosome thermodynamic stability, Biophys. J. 79 (2000) 601–613.
[18] Z. Kam, N. Borochov, H. Eisenberg, Dependence of laser light scattering of DNA on NaCl concentration, Biopolymers 20 (1981) 2671–2690.
[19] E.S. Sobel, J.A. Harpst, Effects of Na^+ on the persistence length and excluded volume of T7 bacteriophage DNA, Biopolymers 31 (1991) 1559–1564.
[20] D. Shore, J. Langowski, R.L. Baldwin, DNA flexibility studied by covalent closure of short fragments into circles, Proc. Natl. Acad. Sci. U. S. A. 78 (1981) 4833–4837.
[21] V. Rizzo, J. Schellman, Flow dichroism of T7 DNA as a function of salt concentration, Biopolymers 20 (1981) 2143–2163.
[22] J.G. Elias, D. Eden, Transient electric birefringence study of the persistence length and electrical polarizability of restriction fragments of DNA, Macromolecules 14 (1981) 410–419.
[23] P.J. Hagerman, Investigation of the flexibility of DNA using transient electric birefringence, Biopolymers 20 (1981) 1503–1535.
[24] S. Diekmann, W. Hillen, B. Morgeneyer, R.D. Wells, D. Pörschke, Orientation relaxation of DNA restriction fragments and the internal mobility of the double helix, Biophys. Chemist. 15 (1982) 263–270.
[25] D. Pörschke, Persistence length and bending dynamics of DNA from electrooptical measurements at high salt concentrations, Biophys. Chemist. 40 (1991) 169–179.
[26] C. Bustamante, J.C. Macosko, G.J.L. Wuite, Grabbing the cat by the tail: manipulating molecules one by one, Nat. Rev., Mol. Cell Biol. 1 (2000) 130–136.
[27] C. Bustamante, S.B. Smith, J. Liphardt, D. Smith, Single-molecule studies of DNA mechanics, Curr. Opin. Struck. Biol. 10 (2000) 279–285.
[28] M. Hegner, W. Grange, Mechanics and imaging of single DNA, J. Muscle Res. Cell Motil. 23 (2002) 367–375.
[29] J. Zlatanova, S.H. Leuba, Stretching and imaging single DNA molecules and chromatin, J. Muscle Res. Cell Motil. 23 (2002) 377–395.
[30] O. Kratky, G. Porod, X-ray investigation of dissolved chain molecules, Recl. Trav. Chim. Pays-Bas Belg. 68 (1949) 1106–1124.
[31] L.D. Landau, E.M. Lifshitz, Statistical Physics, Pergamon Press, London, 1958.
[32] P.J. Flory, Statistical Mechanics of Chain Molecules, John Wiley & Sons, New York, 1969.

[33] J.A. Schellman, The flexibility of DNA, Biopolymers 13 (1974) 217–226.
[34] P.J. Hagerman, Flexibility of DNA, Annu. Rev. Biophys. Biophys. Chem. 17 (1988) 265–286.
[35] E.N. Trifonov, R.K.-Z. Tan, S.C. Harvey, Static persistence length of DNA, in: W.K. Olson, M.H. Sarma, R.H. Sarma, M. Sundaralingam (Eds.), DNA Bending and Curvature, Structure and Expression, vol. 3, Adenine Press, Schenectady, NY, 1988, pp. 243–253.
[36] J.A. Schellman, S.C. Harvey, Static contributions to the persistence length of DNA and dynamic contributions to DNA curvature, Biophys. Chemist. 55 (1995) 95–114.
[37] P. De Santis, M. Fuà, A. Palleschi, M. Savino, Influence of dynamic fluctuations on DNA curvature, Biophys. Chemist. 55 (1995) 261–271.
[38] C. Rivetti, M. Guthold, C. Bustamante, Scanning force microscopy of DNA deposited onto mica: equilibration versus kinetic trapping studied by statistical polymer chain analysis, J. Mol. Biol. 264 (1996) 919–932.
[39] J. Bednar, P. Furrer, V. Katritch, A.Z. Stasiak, J. Dubochet, A. Stasiak, Determination of DNA persistence length by cryo-electron microscopy. Separation of the static and dynamic contributions to the apparent persistence length of DNA, J. Mol. Biol. 254 (1995) 579–594.
[40] L.D. Landau, E.M. Lifshitz, Theory of Elasticity, Pergamon Press, Oxford, NY, 1970.
[41] C. Frontali, E. Dore, A. Ferrauto, E. Gratton, A. Bettini, M.R. Pozzan, E. Valdevit, An absolute method for the determination of the persistence length of native DNA from electron micrographs, Biopolymers 18 (1979) 1353–1357.
[42] G. Muzard, B. Theveny, B. Revet, Electron microscopy mapping of pBR322 DNA curvature. Comparison with theoretical models, EMBO J. 9 (1990) 1289–1298.
[43] B. Theveny, B. Revet, DNA orientation using specific avidin–ferritin biotin end labeling, Nucleic Acids Res. 15 (1987) 947–958.
[44] E.N. Trifonov, Sequence-dependent deformational anisotropy of chromatin DNA, Nucleic Acids Res. 8 (1980) 4041–4053.
[45] V.B. Zhurkin, Sequence-dependent bending of DNA and phasing of nucleosomes, J. Biomol. Struct. Dyn. 2 (1985) 785–804.
[46] C. Rivetti, C. Walker, C. Bustamante, Polymer chain statistics and conformational analysis of DNA molecules with bends or sections of different flexibility, J. Mol. Biol. 280 (1998) 41–59.
[47] J.A.H. Cognet, C. Pakleza, D. Cherny, E. Delain, E. Le Cam, Static curvature and flexibility measurements of DNA with microscopy. A simple renormalization method, its assessment by experiment and simulation, J. Mol. Biol. 285 (1999) 997–1009.
[48] G. Zuccheri, A. Scipioni, V. Cavaliere, G. Gargiulo, P. De Santis, B. Samorì, Mapping the intrinsic curvature and flexibility along the DNA chain, Proc. Natl. Acad. Sci. U. S. A. 98 (2001) 3074–3079.
[49] A. Scipioni, C. Anselmi, G. Zuccheri, B. Samorì, P. De Santis, Sequence-dependent DNA curvature and flexibility from scanning force microscopy images, Biophys. J. 83 (2002) 2408–2418.
[50] A. Scipioni, G. Zuccheri, C. Anselmi, A. Bergia, B. Samorì, P. De Santis, Sequence-dependent DNA dynamics by scanning force microscopy time-resolved imaging, Chem. Biol. 9 (2002) 1315–1321.
[51] B. Sampaolese, A. Bergia, A. Scipioni, G. Zuccheri, M. Savino, B. Samorì, P. De Santis, Recognition of the DNA sequence by an inorganic crystal surface, Proc. Natl. Acad. Sci. U. S. A. 99 (2002) 13566–13570.
[52] C. Anselmi, P. De Santis, R. Paparcone, M. Savino, A. Scipioni, From the sequence to the superstructural properties of DNAs, Biophys. Chemist. 95 (2002) 23–47.
[53] http://www.archimede.chem.uniroma1.it/webdna/.
[54] J. van Noort, T. van der Heijden, M. de Jager, C. Wyman, R. Kanaar, C. Dekker, The coiled-coil of the human Rad50 DNA repair protein contains specific segments of increased flexibility, Proc. Natl. Acad. Sci. U. S. A. 100 (2003) 7581–7586.
[55] P.A. Kitchin, V.A. Klein, K.A. Ryan, K.L. Gann, C.A. Rauch, D.S. Kang, R.D. Wells, P.T. Englund, A highly bent fragment of *Crithidia fasciculata* kinetoplast DNA, J. Biol. Chem. 261 (1986) 11302–11309.
[56] B. Revet, A. Fourcade, Short unligated sticky ends enable the observation of circularised DNA by atomic force and electron microscopies, Nucleic Acids Res. 26 (1998) 2099–2104.
[57] C. Anselmi, P. De Santis, R. Paparcone, M. Savino, A. Scipioni, A possible role of DNA superstructures in genome evolution, Orig. Life Evol. Biosph. 34 (2004) 143–149.
[58] I. Brukner, S. Susic, M. Dlakic, A. Savic, S. Pongor, Physiological concentrations of magnesium ions induces a strong macroscopic curvature in GGGCCC-containing DNA, J. Mol. Biol. 236 (1994) 26–32.
[59] S. Diekmann, Temperature and salt dependence of the gel migration anomaly of curved DNA fragments, Nucleic Acids Res. 15 (1987) 247–265.
[60] V.N. Soyfer, V.N. Potaman, Triple-Helical Nucleic Acids, Springer, New York, 1996.
[61] D.M. Lilley, Structures of helical junctions in nucleic acids, Q. Rev. Biophys. 33 (2000) 109–159.
[62] P.R. Dahlgren, Y.L. Lyubchenko, Atomic force microscopy study of the effects of Mg^{2+} and other divalent cations on the end-to-end DNA interactions, Biochemistry 41 (2002) 11372–11378.
[63] W. Zacharias, J.E. Larson, J. Klysig, S.M. Stirdivant, R.D. Wells, Conditions which cause the right-handed to left-handed DNA conformational transitions. Evidence for several types of left-handed DNA structures in solution, J. Biol. Chem. 257 (1982) 2775–2782.
[64] C.H. Laundon, J.D. Griffith, Cationic metals promote sequence-directed DNA bending, Biochemistry 26 (1987) 3759–3762.
[65] W. Han, M. Dlakic, Y.J. Zhu, S.M. Lindsay, R.E. Harrington, Strained DNA is kinked by low concentrations of Zn^{2+}, Proc. Natl. Acad. Sci. U. S. A. 94 (1997) 10565–10570.
[66] N.C. Seeman, 2004. Nanotechnology and the double helix, Sci. Am. 290 64–69, 72–75
[67] C. Mao, W. Sun, Z. Shen, N.C. Seeman, A nanomechanical device based on the B–Z transition of DNA, Nature 397 (1999) 144–146.
[68] B. Yurke, A.J. Turberfield, A.P.J. Mills, F.C. Simmel, J.L. Neumann, A DNA-fuelled molecular machine made of DNA, Nature 406 (2000) 605–608.
[69] Y. Benenson, T. Paz-Elizur, R. Adar, Z. Livneh, E. Shapiro, Programmable and autonomous computing machine made of bio-molecules, Nature 414 (2001) 430–434.
[70] C.M. Niemeyer, M. Adler, S. Lenhert, S. Gao, H. Fuchs, L.F. Chi, Nucleic acid supercoiling as a means for ionic switching of DNA-nanoparticle networks, ChemBioChem 2 (2001) 260–264.
[71] C.M. Niemeyer, M. Adler, Nanomechanical devices based on DNA, Angew. Chem., Int. Ed. 41 (2002) 3779–3783.
[72] J.W.J. Li, W.H. Tan, A single DNA molecule nanomotor, Nano Lett. 2 (2002) 315–318.
[73] H. Yan, X. Zhang, Z. Shen, N.C. Seeman, A robust DNA mechanical device controlled by hybridization topology, Nature 415 (2002) 62–65.
[74] P. Alberti, J.L. Mergny, DNA duplex–quadruplex exchange as the basis for a nanomolecular machine, Proc. Natl. Acad. Sci. U. S. A. 100 (2003) 1569–1573.
[75] Y. Benenson, R. Adar, T. Paz-Elizur, Z. Livneh, E. Shapiro, DNA molecule provides a computing machine with both data and fuel, Proc. Natl. Acad. Sci. U. S. A. 100 (2003) 2191–2196.
[76] L. Feng, S.H. Park, J.H. Reif, H. Yan, A two-state DNA lattice switched by DNA nanoactuator, Angew. Chem., Int. Ed. Engl. 42 (2003) 4342–4346.
[77] D. Liu, S. Balasubramanian, A proton-fuelled DNA nanomachine, Angew. Chem., Int. Ed. Engl. 42 (2003) 5734–5736.
[78] W. Humphrey, A. Dalke, K. Schulten, VMD—visual molecular dynamics, J. Mol. Graph. 14 (1996) 33–38.